

1 **Different facets of dry/wet patterns in southwestern China over the past**
2 **27,000 years**

3 **Mengna Liao¹ #, Kai Li¹ #, Weiwei Sun², Jian Ni¹**

4 ¹ College of Chemistry and Life Sciences, Zhejiang Normal University, Jinhua, 321004, PR China

5 ² State Key Laboratory of Lake Science and Environment, Nanjing Institute of Geography and Limnology,
6 Chinese Academy of Sciences, Nanjing, 210008, PR China

7 *Correspondence to:* Jian Ni (nijian@zjnu.edu.cn)

8 # Contributing equally.

9

10 **Abstract.** Frequently occurring mega-droughts under current global climate change have
11 attracted broad social attention. A paleoclimatic perspective is needed to increase our
12 understanding of the causes and effects of droughts. Southwestern (SW) China has been
13 threatened by severe seasonal droughts. Our current knowledge of millennial-scale dry and
14 wet phases in this region is primarily based on the variability of the Indian Summer Monsoon.
15 However, water availability over land does not always follow patterns of monsoonal precipitation
16 but also depends on water loss from evaporation and transpiration. Here, we reconstructed
17 precipitation intensity, lake hydrological balance and the soil water stress index (SWSI) for the
18 last 27,000 yr. Grain size, geochemical and pollen records from Yilong Lake reveal the long-
19 term relationships and inconsistencies of dry/wet patterns in meteorological, hydrological and
20 soil systems in central Yunnan region, SW China. Our results show that the long-term trends
21 among precipitation, hydrological balance and soil moisture varied through time. The
22 hydrological balance and soil moisture were primarily controlled by temperature-induced
23 evaporation change during periods of low precipitation such as the Last Glacial Maximum and
24 Younger Dryas. During periods of high precipitation (the early to late Holocene), intensified
25 evaporation from the lake surface offset the effects of increased precipitation on the
26 hydrological balance. However, abundant rainfall and the dense vegetation canopy
27 circumvented a soil moisture deficit that might have resulted from rising temperature. In
28 conclusion, the hydrological balance in central Yunnan region was more sensitive to
29 temperature change while soil moisture could be further regulated by vegetation changes over
30 millennial timescales. Therefore, under future climate warming, the surface water shortage in
31 central Yunnan region may become even more serious. Our study suggests that reforestation
32 efforts may provide some relief to soil moisture deficits in this region.

33

34 1. Introduction

35 The global land area experiencing extreme-to-exceptional terrestrial water storage drought
36 could more than double by the late twenty-first century (Pokhrel et al., 2021). In southwestern
37 (SW) China, drought has become a climate threat which is likely to happen more frequently in
38 the future (Qiu, 2010; Wang et al., 2016). It is generally thought that long-term dry and wet
39 phases in SW China are primarily regulated by the intensity of monsoonal precipitation
40 associated with the evolution of atmospheric circulation systems (Chen et al., 2014; Hillman et
41 al., 2017; Sun et al., 2019; Wang et al., 2019). However, drought refers to the amount of water
42 available in both the soil and hydrological systems which is dependent on precipitation and a
43 range of other factors. These include how much water is able to infiltrate to deeper ground
44 layers or is lost as runoff, and how much is evaporated directly from water and soil surfaces, or
45 transpired by plants (Breshears et al., 2005; Dai et al., 2018; Feng and Liu, 2015; Mishra and
46 Singh, 2010; Trenberth et al., 2014). Therefore, drought doesn't only happen during periods of
47 low precipitation (Dai et al., 2018; Sun et al., 2017; Trenberth et al., 2014; Xu et al., 2019).
48 Given this, understanding dry/wet patterns in different climate scenarios while considering
49 physical and vegetation processes is crucial to predicting the future risk of drought.

50 Climate evolution in SW China since the Last Glacial Maximum (LGM) has been reconstructed
51 using various types of paleoclimatic archives, such as speleothem oxygen isotope records (e.g.,
52 Cai et al., 2015; Dykoski et al., 2005; Zhao et al., 2015), lake sediments (e.g., Hillman et al.,
53 2017; Hillman et al., 2020; Hodell et al., 1999; Li et al., 2018; Sun et al., 2019; Wang et al.,
54 2020; Wu et al., 2018; Xiao et al., 2014a; Xiao et al., 2014b; Zhang et al., 2017; Zhang et al.,
55 2019a), and peats (e.g., Huang et al., 2016; Wei et al., 2012). The major conclusion of these
56 studies is that monsoonal precipitation and temperature was very low during the LGM,
57 precipitation peaked in the early Holocene during a period of warmer climate, before both
58 precipitation and temperature declined. The "cold-dry" and "warm-humid" paradigms of climate
59 change in SW China have been widely demonstrated from a paleoclimatological perspective,
60 despite the proposition that summer temperature and monsoon precipitation were decoupled
61 in the early Holocene (Wu et al., 2018). Additionally, vegetation in SW China has experienced
62 noticeable changes since the LGM (Chen et al., 2014; Cook et al., 2011; Wu et al., 2018; Xiao

63 et al., 2014a; Xiao et al., 2014b), which may have affected evapotranspiration processes. Since
64 water availability is a trade-off among precipitation input and water loss through evaporation,
65 transpiration and outflow (Breshears et al., 2005; Dai et al., 2018; Watras et al., 2014), these
66 processes may lead to different environmental signatures of the wet and dry patterns over land.
67 However, to our knowledge few studies have tested this idea.

68 Definitions of “drying” in meteorology, hydrology and biology are different but connected
69 (Mishra and Singh, 2010). In paleoclimatology, drying or moistening processes can be
70 reconstructed by different types of proxies, but the concepts underpinning them are not
71 necessarily the same. For example, grain-size records from several lakes in SW China reflected
72 variations in Indian Summer Monsoon (ISM) precipitation (Ning et al., 2017; Peng et al., 2019;
73 Sheng et al., 2015). Authigenic carbonate precipitation is strongly affected by the hydrological
74 balance or precipitation/evaporation ratio (Leng and Marshall, 2004; Ohlendorf et al., 2013),
75 and thus indicates changing hydrological conditions in lake-catchment systems. For terrestrial
76 ecosystems, soil water is the main and direct source of water for most plants and a primary
77 constraint for vegetation composition and biomass. Consequently, changes in the soil moisture
78 can theoretically be reflected in pollen records. As yet, soil moisture status has rarely been
79 reconstructed using pollen data, and the similarities and differences between the dry/wet
80 patterns revealed from different paleoproxies are seldom discussed.

81 The Yunnan region is located in the SW of China (Fig. 1). It is primarily influenced by warm and
82 humid airflow from the Bay of Bengal in summer. Several paleolimnological studies have shown
83 that, since the LGM or the Holocene, precipitation, hydrological conditions and vegetation in
84 the Yunnan region has experienced noticeable changes (Hillman et al., 2017; Hillman et al.,
85 2020; Hodell et al., 1999; Ning et al., 2017; Sun et al., 2019; Wu et al., 2018; Xiao et al., 2014a).
86 However, few studies have applied a multi-proxy approach at the same temporal scale to
87 explore different aspects of the long-term dry/wet patterns. Here we have developed the first
88 record of soil water stress index (SWSI) based on a pollen record from Yilong Lake in the
89 Yunnan region to reveal changes in soil moisture over the past 27,000 years. By comparing the
90 SWSI reconstruction with records of monsoonal precipitation and hydrological balance in the

91 same core, we aim to discuss the long-term relationships of dry/wet patterns in the
92 meteorological, hydrological and soil systems in SW China.

93 **2. Materials and methods**

94 2.1 Study site and modern climate

95 Yilong Lake (23.63–23.70° N, 102.50–102.65° E, 1414 m a.s.l.) is a faulted lake in central
96 Yunnan region, SW China (Fig. 1a). It covers an area of 38 km² and has a catchment area of
97 303.6 km² (Wang and Dou, 1998). The average water depth is 2.8 m and the maximum is 6.2
98 m (Wang and Dou, 1998). Yilong Lake is a freshwater lake which is fed by overland runoff, lake
99 surface precipitation and groundwater. All the inflowing rivers, except the Chenghe River at the
100 northwest of the Lake, are seasonal (Fig. 1b). An outlet was located at the southeast end of the
101 lake during past highstands, but it disappeared in 1978 CE due to climate- and human-induced
102 lower lake levels (Wang and Dou, 1998).

103 The central Yunnan region is dominated by a subtropical monsoon climate. Observations from
104 the closest meteorological station in Yuxi City (24.2° N, 102.338° E, 1717 m a.s.l.), 80 km away
105 from Yilong Lake, record a mean annual temperature of 18.1 °C after lapse rate correction
106 (0.65 °C per 100 m) and mean annual precipitation of 886 mm (1951–2017 CE; China
107 Meteorological Data Service Centre, <https://data.cma.cn/en>). Annual evaporation (1035 mm) in
108 this region is slightly higher than the annual precipitation. Seasonal climate change is
109 characterized by high precipitation in the warm season with low precipitation in the cold season
110 (Fig. 1c).

111 2.2 Sampling and dating

112 In May 2017, a sediment core (YLH) was retrieved from Yilong Lake at a water depth of 4.1 m
113 (Fig. 1b) using a UWITEC sampling system. The sediment core was transported to the School
114 of Geography, Nanjing Normal University laboratory and kept at 3.9 °C until analysis. The
115 sediment core was split with a Geotek Core Splitter, photographed and visually described in
116 the laboratory. The samples were subsampled at 1-cm intervals, freeze-dried, and used for

117 further analyses.

118 The age of the core YLH was determined using fifteen accelerator mass spectrometry (AMS)
119 ¹⁴C dates including bulk organic matter, charcoal and plant remains (Table 1). ¹⁴C dates were
120 analysed by the Beta Analytic Testing Laboratory. The conventional ¹⁴C dates were calibrated
121 using Calib 8.20 with an IntCal20 calibration dataset (Reimer et al., 2020). Age-depth modelling
122 was performed in R (version 3.4.4, R Core Team, 2018) using the package “rbacon” (Blaauw
123 et al., 2020). According to the age-depth model, the basal sediment was deposited between
124 27.171–26.439 cal. ka BP with a median age of 26.866 cal. ka BP (Fig. 2).

125 2.3 Analytical methods

126 Samples for grain size analysis were measured at 1-cm intervals. All samples were pretreated
127 with 30 % H₂O₂ and then 5 % HCl to remove organic matter and carbonates, rinsed with
128 deionized water to neutralize the samples, and placed in an ultrasonic bath with 10 % (NaPO₃)₆
129 added to disperse particles. The grain size distribution was measured by a Malvern 3000E laser
130 diffraction instrument with 100 bins ranging from 0.02 to 2000 μm.

131 The sediments (collected at 1-cm intervals) were pretreated with 10 % HCl to remove
132 carbonates and then used to measure the total organic carbon (TOC) and total nitrogen (TN)
133 using a vario EL cube Elemental Analyzer. Replicate analyses of well-mixed samples showed
134 that the precision was ca. ± <0.1 % (1 standard deviation (s.d.)). Continuous down-core X-ray
135 fluorescence (XRF) measurements of the geochemical composition were carried out with a
136 core scanner (MSCL-S Specifications; tube voltage 15 kV, exposure time 30 s and spatial
137 distribution 0.5) at the laboratory of the School of Geography, Nanjing Normal University. The
138 sample moved along a monochromatized and polarized SR beam. Core scanning started from
139 10 cm depth as the upper 10 cm of sediments has a high water content and are too soft to get
140 robust measurements. Core bulk mineralogy of freeze-dried and milled samples (at 2-cm
141 intervals) were measured by X-ray diffraction (XRD) using a PANalytical X’pert Pro (40 kV, 30
142 mA, from 5 to 80°, step-rate 0.0167°, Cu Kα radiation) at the Qinghai Institute of Salt Lakes,
143 Chinese Academy of Science (CAS). A total of 71 freeze-dried samples from depths where

144 carbonate content is (relatively) high (10–176 cm and 228–280 cm) were measured for oxygen
145 stable isotopes in carbonate ($^{18}\text{O}_{\text{carb}}$) using a Thermo-Fisher MAT 253 mass spectrometer
146 equipped with a Kiel-IV carbonate preparation device at the Nanjing Institute of Geography and
147 Limnology, CAS. The samples were pretreated with 100 % phosphoric acid. The $^{18}\text{O}_{\text{carb}}$ values
148 are expressed as standard delta (δ) notation as the per mil (‰) deviation from Vienna Pee Dee
149 Belemnite (VPDB). Four samples at different depths were imaged using a Hitachi SU8010
150 scanning electron microscope (SEM) to examine crystal structure and morphology of carbonate
151 minerals.

152 Samples for pollen analysis were analysed at 4-cm intervals and treated standard laboratory
153 methods (Faegri et al., 1989), including treatment with 10 % HCl and 50 % HF to remove
154 carbonates and silicates, boiling in 10 % KOH to remove humic acid, sieving to remove the fine
155 and coarse fractions, and mounting in silicone oil. To calculate the concentrations of pollen,
156 tablets containing a known quantity of *Lycopodium* spores were added to each sample prior to
157 the treatments. At least 300 terrestrial pollen grains per sample were counted. All the treatment
158 and identification was processed in the Institute of Hydrogeology and Environmental Geology,
159 Chinese Academy of Geological Sciences. The pollen percentages were calculated based on
160 the total number of pollen grains from terrestrial pollen taxa and used to construct a pollen
161 diagram and conduct numerical analyses.

162 2.4 Pollen-based quantitative reconstruction of SWSI

163 In total, 1394 surface soil pollen samples from SW China (Ni et al., 2014; Fig. S1 in the
164 Supplement) were used in this study. Annual climate data was averaged from long-term records
165 from 1971 to 2000 at 1814 meteorological stations across China (China Meteorological Data
166 Service Centre, <https://data.cma.cn/en>). These data were interpolated into 1 km grid cells using
167 a thin plate smoothing spline surface fitting technique (Hancock and Hutchinson, 2006) that
168 takes the impact of elevation into account on the basis of the Shuttle Radar Topography Mission
169 (SRTM) digital elevation model (Farr et al., 2007). The interpolation was performed in the
170 program ANUSPLIN version 4.36 (Hutchinson, 2006). The interpolated meteorological data
171 were used to calculate the SWSI using the SPLASH v.1.0 program (Davis et al., 2017). SWSI

172 reflects the degree of evapotranspiration deficit and is expressed as $(PET-AET)/PET$, where
173 AET and PET are the annual sums of actual and potential evapotranspiration, respectively
174 (Prentice et al., 1993). The SWSI reconstruction was calculated using the weighted-averaging
175 partial least square (WA-PLS) regression (ter Braak and Juggins, 1993). The pollen
176 percentages were square-root transformed to stabilize variances and optimize the signal-to-
177 noise ratio (Prentice, 1980). The 'leave-one-out' cross-validation was used to test the reliability
178 and robustness of the model. The number of components to include in the transfer function was
179 selected as those producing the lowest root mean squared error of prediction (*RMSEP*), a high
180 coefficient of determination between observed and predicted environmental values (r^2) and low
181 average bias (ter Braak and Juggins, 1993). These analyses were carried out using R package
182 "rioja" (Juggins, 2017).

183 **3. Results**

184 3.1 Grain size and geochemical data of core YLH

185 Grain size in core YLH are mainly composed of clay ($< 4 \mu\text{m}$) and silt ($4\text{--}63 \mu\text{m}$), with mean
186 contributions of 25 % and 70.2 %, respectively. Down-core variations of the clay component
187 exhibit generally high values during ca. 16–27.5 cal. ka BP (ca. 246–456 cm) and ca. 0–3 cal.
188 ka BP (ca. 0–40 cm), and low values with strong fluctuations during ca. 3–16 cal. ka BP (ca.
189 41–245 cm) (Fig. 3). The variations of the silt component are generally opposite to that of the
190 clay component. The sand component is characterized by low percentages throughout the core
191 (average percentage of 4.8 %), punctuated by two intervals (ca. 3–5 cal. ka BP and ca. 13–16
192 cal. ka BP) with a slight increase (average ca. 8–10 %) (Fig. 3). The median size was small
193 during ca. 15–27.5 cal. ka BP (ca. 235–456 cm) and ca. 0–2 cal. ka BP (ca. 0–26 cm). In the
194 period of 2–15 cal. ka BP, the median size was relatively big but around 11 cal. ka BP, it is as
195 small as that in other periods (Fig. 3).

196 TOC within the samples varies between 0.75 % and 15.13 %, and TN varies from 0.08 % to
197 2.01 % (Fig. 3). TOC increases from 9 % to 15 % between 27.5–20 cal. ka BP and then
198 decreases to 5 % around 12–9 cal. ka BP. A sudden increase in TOC to 10–14 % occurs after

199 9 cal. ka BP and then decreases sharply to 0.75 % between 5–3 cal. ka BP before increasing
200 again (Fig. 3). Variations in TN and TOC are highly synchronous (Fig. 3). The C/N ratio is around
201 10 during 27.5–13 cal. ka BP and higher than 10 during 8–7 and 5–3 cal. ka BP, with lower than
202 10 during 13–8, 7–5 and 3–0 cal. ka BP (Fig. 3). The Fe/Mn ratio peaks around 13–9 cal. ka
203 BP (Fig. 3).

204 XRD detects quartz, calcite, aragonite, magnetite, muscovite, gypsum, rhodochrosite, dolomite,
205 clinocllore as major minerals in the core sediments. Carbonate in the core appears primarily
206 in two sections, between 0–180 cm and 226–288 cm (Fig. 3). Aragonite exists only in the upper
207 34-cm sediments, which partially compensates for the decrease of calcite (Fig. 3). The $\delta^{18}\text{O}_{\text{carb}}$
208 varies from -8.435 ‰ to -2.525 ‰ during 18 to 14.5 cal. ka BP and from -10.472 ‰ to -4.371 ‰
209 during 8.5–0.77 cal. ka BP (Fig. 3). $^{18}\text{O}_{\text{carb}}$ enriched consistently since 8.5 cal. ka BP (Fig. 3).

210 3.2 Pollen assemblage variations and reconstructed SWSI over the past 27,000 years

211 A total of 99 pollen taxa were identified in 114 samples. Pollen from tree taxa, including *Pinus*,
212 *Picea*, evergreen and deciduous *Quercus* (*Quercus.Eve* and *Quercus.Dec*), *Betula* and *Tsuga*,
213 dominated the entire pollen record, with an average percentage of 85.6 % (Fig. 4). The shrub
214 taxa only accounts for 1.08 % of the entire pollen record. The average percentage of the
215 herbaceous taxa is 13.3 %. Among the herb taxa, only *Artemisia*, Poaceae and Asteraceae
216 have average percentages >1 %. Herbs increased abruptly for several brief time intervals
217 between 8–6 cal. ka BP and between 3–2 cal. ka BP (Fig. 4). The most noticeable change in
218 the tree pollen composition occurred around 13 cal. ka BP, when *Quercus.Dec* was replaced
219 rapidly by *Quercus.Eve* and *Betula*, and the coniferous taxa (*Abies*, *Picea*, *Pinus* and *Tsuga*)
220 almost disappeared (Fig. 4). Another obvious change in the pollen composition occurred at 3
221 cal. ka BP, when *Pinus*, *Artemisia* and Poaceae increased considerably, and *Quercus.Eve*,
222 *Quercus.Dec*, *Betula* and *Alnus* decreased. The average percentage of herbs was relatively
223 low compared with woody plants throughout the core. But the abundance of herbaceous pollen
224 increased noticeably between 8–6 cal. ka BP and especially after 3 cal. ka BP, with the
225 maximum percentage more than 90 %.

226 A two-component WA-PLS model was selected on the basis of high r^2 (0.62), low *RMSEP*
227 (0.159) and the smallest number of ‘useful’ components (Table S1 in the Supplement). High
228 (low) SWSI values indicates large (small) water stress in soil system. The reconstructed SWSI
229 ranges from 0 to 0.29, reflecting low to moderate water stress over the past 27,000 years.
230 Relatively high SWSI occurred in three periods: 20–15 cal. ka BP, 8–6 cal. ka BP and 4–0 cal.
231 ka BP (Fig. 4).

232 **4. Discussion**

233 4.1 Precipitation change revealed by grain size

234 The grain size composition of lake sediments contains information on the sources of clastic
235 materials, lake level fluctuations and transport energy related to variations in runoff (Peng et al.,
236 2005; Xiao et al., 2013). A previous study on the spatial characteristics of grain-size distributions
237 in the surface sediments of Yilong Lake revealed that, as the water depth decreased, the
238 median size increased and the grain-size distribution curve changed from “unimodal” to
239 “bimodal” (Zhang et al., 2019b). Yilong Lake is located in the realm of the ISM, where the source
240 of clastic materials (especially coarse particles) and the transport energy are primarily
241 controlled by precipitation. An increase in precipitation not only enhances the erosion intensity
242 of the basin, but also increases the runoff, which will lead to the transportation of more coarse
243 particles into the lake. In the core YLH, most of the samples with a relatively large median grain
244 size show a “unimodal” distribution (Fig. S2 in the Supplement), which implies a relatively high
245 lake level and an increase in precipitation-transported coarse particles into the central part of
246 the lake. Consequently, an increase in the sand component and median grain size coarsening
247 should relate to intensified hydrological energy under increased precipitation.

248 Carbonate deposited from the lake water was assumed to preserve the $\delta^{18}\text{O}$ signal of
249 precipitation and hence the $\delta^{18}\text{O}_{\text{carb}}$ from lake sediments is a good proxy for reflecting
250 precipitation intensity or ISM in the Yunnan region (Hillman et al., 2017; Hillman et al., 2020;
251 Hodell et al., 1999; Sun et al., 2019). A moderately strong negative correlation between
252 precipitation $\delta^{18}\text{O}$ and monthly precipitation amount at Kunming, SW China, has been reported

253 (Hillman et al., 2017). Therefore, the assumption that the $\delta^{18}\text{O}$ of the water in Yilong Lake was
254 controlled by the $\delta^{18}\text{O}$ of precipitation is reasonable. The changes in the median grain size in
255 core YHL closely match that of $\delta^{18}\text{O}_{\text{carb}}$, with the small grain size corresponding to high $\delta^{18}\text{O}_{\text{carb}}$
256 values, and vice versa (Fig. 5). This supports the theory that the median grain size is a reliable
257 indicator of precipitation intensity in Yilong Lake. However, it should be noted that grain-size
258 data from the samples in the last 3,000 years cannot be simply interpreted as changes in
259 precipitation intensity because human activities strongly affected the regional landscape and
260 freshwater systems during this period (Wu et al., 2015; Xiao et al., 2017).

261 Variations of the median grain size from core YLH reflect less monsoonal precipitation during
262 ca. 27–15 cal. ka BP and generally high precipitation between ca. 15–3 cal. ka BP (Fig. 5). This
263 pattern is generally consistent with many lines of evidence from stalagmites (Cai et al., 2015;
264 Cheng et al., 2016; Dykoski et al., 2005; Zhao et al., 2015) and lake sediments (Hodell et al.,
265 1999; Peng et al., 2019; Sun et al., 2019). Additionally, variations of the median grain size also
266 record the well-known climatic events Bølling/Allerød (B/A) and Younger Dryas (YD), shown
267 respectively as a sharp increase and decrease in the monsoonal precipitation (Fig. 4). The
268 occurrence time of the B/A event recorded in this study is consistent with that documented in
269 the stalagmite $\delta^{18}\text{O}$ records from Cave Dongge (Dykoski et al., 2005), Sanbao (Cheng et al.,
270 2016) and Xiaobailong (Cai et al., 2015) (Fig. 5). However, the YD event in this study lagged
271 ca. 1,000 years behind that recorded in the stalagmite $\delta^{18}\text{O}$ from Cave Dongge (Dykoski et al.,
272 2005) and Sanbao (Cheng et al., 2016). This delayed monsoon signal is recorded in the
273 stalagmite $\delta^{18}\text{O}$ record from Xiaobailong Cave (Cai et al., 2015) which is only ca. 85 km away
274 from Yilong Lake. Understanding the mechanisms driving this lag is beyond the scope of this
275 study, but uneven rainfall distribution due to the complex topography of the Yunnan-Guizhou
276 Plateau likely played an important role.

277 4.2 Carbonate deposition as a record of past hydrological balance

278 Carbonate deposition in Yilong Lake is mainly composed of autochthonous calcite and
279 aragonite (Fig. S3 in the Supplement). A large number of mollusk shells are the main source of
280 the aragonite that only appears in the upper 34-cm of the core. Autochthonous calcite

281 precipitation needs a certain degree of supersaturation (Raidt and Koschel, 1988) which can
282 be achieved by seasonal temperature increase and plankton flourishing (Robbins and
283 Blackwelder, 1992; Stabel, 1986). ¹⁸O measurements of the lake water and precipitation
284 indicated significant evaporative effects in Yilong basin during the warm season (Whitmore et
285 al., 1997). Increased temperature exerts a direct control on water evaporation, which will
286 concentrate dissolved carbonates and hence facilitate carbonate precipitation. Photosynthesis
287 of plankton influences carbonate precipitation by affecting CO₂ and pH in the epilimnetic water
288 and/or providing nucleation sites for crystallization (Robbins and Blackwelder, 1992; Stabel,
289 1986). Assuming that lake primary productivity played a big role in carbonate precipitation,
290 algae productivity should have increased during 20–14 cal. ka BP when carbonate content
291 increased, and decreased during 14–9 cal. ka BP when carbonate content decreased. But in
292 fact, relatively high C/N values between 20–14 cal. ka BP and low values between 14–9 cal. ka
293 BP indicate relatively low and high algae productivity, respectively. In addition, characteristics
294 of the crystal morphology of calcite also indicate abiotic origins (Fig. S3 in the Supplement).
295 Consequently, lake primary productivity is not a main cause for carbonates precipitated in
296 Yilong Lake. The carbonate content in the lake sediments should reflect the hydrological
297 balance (i.e. P-E).

298 The variations of the carbonate content in the lake sediments (Fig. 3) indicate a relatively
299 positive water balance between 27–20 cal. ka BP and 14–9 cal. ka BP, and a negative water
300 balance between 20–14 cal. ka BP and 9–0 cal. ka BP. Carbonate records from the two nearby
301 shallow Lakes Xingyun and Qilu (Fig.1, Hillman et al., 2017; Hillman et al., 2020; Hodell et al.,
302 1999) show broadly similar patterns to this record, indicating that the hydrological changes
303 reconstructed in this study reflect a regional rather than a local climate signal.

304 4.3 Different patterns of long-term changes in precipitation, hydrological balance and SWSI, 305 and the potential mechanisms

306 Precipitation is the primary source of water for lacustrine systems and soils. It is generally
307 assumed that dry conditions occurred when precipitation was low, and wet conditions prevailed
308 when precipitation was high. From this point of view, we may conclude that our study region

309 experienced “dry” conditions during the cold LGM and a “wet” phase during the warm Holocene.
310 This pattern generally agrees with other paleoclimate reconstructions from the Yunnan region
311 (e.g., Cheng et al., 2016; Xiao et al., 2014b). However, it does not match well with the
312 hydrological balance and SWSI reconstructions from the same core. This study finds that during
313 the LGM (27–20 cal. ka BP) and the YD event, precipitation was low but the water balance of
314 Yilong Lake was positive and the soil moisture was relatively high. During the early to late
315 Holocene (9–3 cal. ka BP), precipitation was high but the water balance was negative. The
316 definition of dryness is the shortage of available water, which is fundamentally a trade-off
317 between water input and output (Breshears et al., 2005; Dai et al., 2018; Mishra and Singh,
318 2010; Trenberth et al., 2014; Watras et al., 2014). Therefore, factors controlling water loss from
319 terrestrial systems can also play a large role in the creation of dry conditions.

320 Evaporation is one of the important pathways by which water is lost from terrestrial
321 environments. The evaporation rate is higher at higher temperatures because the average
322 kinetic energy of the water molecules increases and more can fly off the surface. Our pollen
323 record revealed that *Quercus*.Dec and the coniferous taxa were rapidly replaced by
324 *Quercus*.Eve and *Betula* around 13 cal. ka BP (Fig. 3). According to the Vegetation Map of the
325 People’s Republic of China (The Editorial Committee of Vegetation Map of China, CAS, 2007),
326 deciduous broad-leaved forest is distributed in areas with lower temperature compared to
327 evergreen broad-leaved forest. Therefore, the characteristics of the pollen compositional
328 change during the transition from glacial to post-glacial period reflects rising temperature. The
329 LGM was characterized by low temperature under which the simulated annual-mean potential
330 evapotranspiration decreased by 10–40 % over nearly all land (Scheff et al., 2017). Decreasing
331 evaporation is a major driver of increasing effective summer moisture availability which has a
332 profound influence on the hydrological states of lakes (Aichner et al., 2019). These factors can
333 explain the positive hydrological balance and relatively wet soils reconstructed during the LGM.
334 The precipitation during 20–15 cal. ka BP was as low as the previous period while insolation
335 was increasing (Fig. 5). Our pollen record showed an obvious decrease in *Picea*, indicating a
336 warmer climate during 20–15 cal. ka BP than in the previous period. This period corresponds
337 to the late glacial warming which is widely reported in the Yunnan region (Fig. 5, Wang et al.,

338 2020; Xiao et al., 2014b; Zhang et al., 2019a). The increased temperature would intensify
339 evaporation and lead to water deficiency in lacustrine and soil environments. Therefore, the
340 hydrological and soil drying during 20–15 cal. ka BP should be triggered by increasing
341 temperatures. However, in spite of the high temperature, soil moisture was still relatively high
342 during 9–3 cal. ka BP (Fig. 5). Water loss from soil systems is more complex than that from free
343 water surfaces because both temperature and the underlying surface conditions affect the ways
344 and the amount of soil water loss or soil water storage capacity (Maxwell and Condon, 2016;
345 Zhang and Schilling, 2006).

346 Water is distributed across the landscape during a rainfall event, with precipitation intercepted
347 by foliage, stored in the soil profile or collected in groundwater aquifers. The amount of water
348 stored in soil profiles and aquifers can be regulated by plant processes (Guzha et al., 2018;
349 Mohammad and Adam, 2010). Previous studies have shown that, both at a stand level and at
350 a global scale, plant transpiration accounts for the largest portion of the total evapotranspiration
351 ($61\% \pm 15\% \text{ s.d.}$ – $64\% \pm 13\% \text{ s.d.}$, Good et al., 2015; Maxwell and Condon, 2016; Schlesinger
352 and Jasechko, 2014). Our results show that the pollen concentration was high during 9–3 cal.
353 ka BP. Although there isn't an obvious linear correlation between pollen concentration and
354 vegetation cover (Luo et al., 2009; Xu et al., 2007), a three-fold increase in the average pollen
355 concentration from the late Pleistocene to Holocene period can be interpreted as a relatively
356 large change in the plant biomass through time. An increase in aboveground biomass likely
357 increased the vegetation canopy and root biomass density (Cairns et al., 1997), causing more
358 water loss from deeper soil layers and aquifers by transpiration through leaf stomata, rather
359 than evaporative loss directly from shallow soil (Lawrence and Slingo, 2004; Markewitz et al.,
360 2010). The abundant precipitation and denser canopy cover in the early to middle Holocene
361 resulted in a period of higher soil moisture availability, despite increasing temperatures and
362 plant biomass likely causing an increase in the total evapotranspiration at this time.

363 The results of this study show that over the recent 3,000 years the meteorological, hydrological
364 and soil systems were all in a dry phase (Fig. 5). At the same time, human activities had
365 intensified and changed the underlying surface conditions in the Yunnan region (Xiao et al.,

366 2017; Xiao et al., 2018). *Pinus* sp. are typically pioneer species, which can colonize disturbed
367 sites if competition and grazing pressures are low. Increases in Poaceae pollen abundance is
368 commonly interpreted as reflecting increased regional aridity, but it is also influenced by early
369 farming activities. If climate change was the only critical cause for vegetation change during the
370 last 3,000 years, the vegetation composition should have changed to a status similar to that
371 recorded in the previous “cool-dry” period. However, the results of the cluster analysis show
372 that samples from the last 3,000 years appear across all three clusters identifying the late
373 glacial period, early Holocene and mid- to late Holocene (Fig. S4 in the Supplement). Therefore,
374 the pollen-based SWSI may have failed to reflect the real soil moisture condition for the recent
375 3,000 years. At present, we cannot estimate the impacts and effects of human activities on lake
376 hydrologic regimes and watershed landscapes in this period. Thus, producing an accurate
377 reconstruction of the monsoonal precipitation, hydrological balance and soil moisture for the
378 past 3,000 years is limited.

379 **5. Conclusions**

380 Sedimentological and pollen data from Yilong Lake provide a 27,000-yr perspective of local and
381 regional variations in the ISM precipitation, hydrological balance and soil moisture condition in
382 SW China. The results show that the reconstructed precipitation is generally consistent with the
383 regional pattern, with low precipitation during the LGM and the YD event and high precipitation
384 during the B/A event and the early to middle Holocene. But since the LGM, the long-term
385 changes in precipitation, hydrological balance and soil moisture are not completely consistent.
386 On a millennial scale, the hydrological balance was more sensitive to temperature change
387 which directly controls the lake surface evaporation rate. In addition to precipitation and
388 temperature, plant processes may also play a large role in regulating soil moisture. Plant
389 biomass in the Yilong area increased during the early to middle Holocene as recorded in the
390 pollen records. This likely increased the vegetation canopy, causing less water loss from
391 shallow soil via evaporation. Human activities intensified during the last 3,000 years. It is difficult
392 to estimate the impact of human activities on the regional landscape and on the watershed
393 hydrology in SW China in the late Holocene. Therefore, the reconstructed deficit in the
394 hydrological and soil systems during this period cannot be interpreted simply as climate change.

395 Finally, our study highlights that “wetness” and “dryness” should be precisely defined when
396 interpreting different paleoproxies.

397 **Data availability**

398 The reconstructed data presented in the paper can be accessed by contacting Mengna Liao or
399 Jian Ni.

400 **Author contributions**

401 ML, KL and JN developed the research questions. ML, KL and WS designed and conducted
402 the experiment. KL conducted the fieldwork. ML, KL, WS analysed samples and processed
403 data. ML and KL wrote the manuscript with contributions from all co-authors.

404 **Competing interests**

405 The authors declare that they have no conflict of interest.

406 **Acknowledgements**

407 This study was supported by the National Basic Research Program of China
408 (2016YFC0502101), the Strategic Priority Research Program of the Chinese Academy of
409 Sciences (XDA2009000003), the Strategic Priority Research Program of Chinese Academy of
410 Sciences (XDB40000000) and the funding from Nanjing Institute of Geography and Limnology,
411 Chinese Academy of Sciences (2021NIGLAS-CJH03). We appreciated Hongbo Zheng and
412 Zhujun Hu from Nanjing Normal University for their help with the XRF core-scanning, Shijie Li
413 from Institute of Geochemistry, CAS for field sampling, and Lydia Lattin Mackenzie from
414 Zhejiang University for language editing.

415 **References**

- 416 Ahn, J., Wahlen, M., Deck, B. L., Brook, E. J., Mayewski, P. A., Taylor, K. C., and White, J. W.: A record of
417 atmospheric CO₂ during the last 40,000 years from the Siple Dome, Antarctica ice core, *J. Geophys.*
418 *Res.-Atmos.*, 109, D13305, <https://doi.org/10.1029/2003JD004415>, 2004.
- 419 Aichner, B., Makhmudov, Z., Rajabov, I., Zhang, Q., Pausata, F. S., Werner, M., Heinecke, L., Kuessner,

420 M. L., Feakins, S. J., and Sachse, D.: Hydroclimate in the Pamirs was driven by changes in
421 precipitation-evaporation seasonality since the Last Glacial Period, *Geophys. Res. Lett.*, 46, 13972–
422 13983, <https://doi.org/10.1029/2019GL085202>, 2019.

423 Blaauw, M., Christen, J. A., and L., M. A. A.: rbacon: Age-depth modelling using Bayesian statistics. R
424 package version 2.5.0. [code], <https://CRAN.R-project.org/package=rbacon>, 2020.

425 Breshears, D. D., Cobb, N. S., Rich, P. M., Price, K. P., Allen, C. D., Balice, R. G., Romme, W. H., Kastens,
426 J. H., Floyd, M. L., and Belnap, J.: Regional vegetation die-off in response to global-change-type
427 drought, *P. Natl. Acad. Sci. USA*, 102, 15144–15148, <https://doi.org/10.1073/pnas.0505734102>, 2005.

428 Cai, Y., Fung, I. Y., Edwards, R. L., An, Z., Cheng, H., Lee, J.-E., Tan, L., Shen, C.-C., Wang, X., and Day,
429 J. A.: Variability of stalagmite-inferred Indian monsoon precipitation over the past 252,000 y, . *Natl.*
430 *Acad. Sci. USA*, 112, 2954–2959, <https://doi.org/10.1073/pnas.1424035112>, 2015.

431 Cairns, M. A., Brown, S., Helmer, E. H., and Baumgardner, G. A.: Root biomass allocation in the world's
432 upland forests, *Oecologia*, 111, 1–11, <https://doi.org/10.1007/s004420050201>, 1997.

433 Chen, X., Chen, F., Zhou, A., Huang, X., Tang, L., Wu, D., Zhang, X., and Yu, J.: Vegetation history,
434 climatic changes and Indian summer monsoon evolution during the Last Glaciation (36,400–13,400
435 cal yr BP) documented by sediments from Xingyun Lake, Yunnan, China, *Palaeogeogr. Palaeocl.*,
436 410, 179–189, <https://doi.org/10.1016/j.palaeo.2014.05.027>, 2014.

437 Cheng, H., Edwards, R. L., Sinha, A., Spötl, C., Yi, L., Chen, S., Kelly, M., Kathayat, G., Wang, X., and Li,
438 X.: The Asian monsoon over the past 640,000 years and ice age terminations, *Nature*, 534, 640–646,
439 <https://doi.org/10.1038/nature18591>, 2016.

440 Cook, C. G., Jones, R. T., Langdon, P. G., Leng, M. J., and Zhang, E.: New insights on Late Quaternary
441 Asian palaeomonsoon variability and the timing of the Last Glacial Maximum in southwestern China,
442 *Quaternary Sci. Rev.*, 30, 808–820, <https://doi.org/10.1016/j.quascirev.2011.01.003>, 2011.

443 Dai, A., Zhao, T., and Chen, J.: Climate change and drought: A precipitation and evaporation perspective,
444 *Curr. Clim. Change Rep.*, 4, 301–312, <https://doi.org/10.1007/s40641-018-0101-6>, 2018.

445 Davis, T., Prentice, I. C., Stocker, B., Thomas, R., Whitley, R., Wang, H., Evans, B., Gallego-Sala, A.,
446 Sykes, M., and Cramer, W.: Simple process-led algorithms for simulating habitats (SPLASH v. 1.0):
447 robust indices of radiation, evapotranspiration and plant-available moisture, *Geosci. Model Dev.*, 10,
448 689–708, <https://doi.org/10.5194/gmd-10-689-2017>, 2017.

449 Dykoski, C. A., Edwards, R. L., Cheng, H., Yuan, D., Cai, Y., Zhang, M., Lin, Y., Qing, J., An, Z., and

450 Revenaugh, J.: A high-resolution, absolute-dated Holocene and deglacial Asian monsoon record from
451 Dongge Cave, China, *Earth Planet. Sc. Lett.*, 233, 71–86, <https://doi.org/10.1016/j.epsl.2005.01.036>,
452 2005.

453 Faegri, K., Kaland, P. E., and Krzywinski, K.: *Textbook of pollen analysis*, John Wiley & Sons Ltd.,
454 Chichester, United Kingdom, 1989.

455 Farr, T. G., Rosen, P. A., Caro, E., Crippen, R., Duren, R., Hensley, S., Kobrick, M., Paller, M., Rodriguez,
456 E., Roth, L., Seal, D., Shaffer, S., Shimada, J., Umland, J., Werner, M., Oskin, M., Burbank, D., and
457 Alsdorf, D.: The shuttle radar topography mission, *Rev. Geophys.*, 45, Art. No. RG2004,
458 <https://doi.org/10.1029/2005RG000183>, 2007.

459 Feng, H. and Liu, Y.: Combined effects of precipitation and air temperature on soil moisture in different
460 land covers in a humid basin, *J. Hydrol.*, 531, 1129–1140,
461 <https://doi.org/10.1016/j.jhydrol.2015.11.016>, 2015.

462 Good, S. P., Noone, D., and Bowen, G.: Hydrologic connectivity constrains partitioning of global terrestrial
463 water fluxes, *Science*, 349, 175–177, <https://doi.org/10.1126/science.aaa5931>, 2015.

464 Guzha, A., Rufino, M. C., Okoth, S., Jacobs, S., and Nóbrega, R.: Impacts of land use and land cover
465 change on surface runoff, discharge and low flows: Evidence from East Africa, *J. Hydrol.-Reg. Stud.*,
466 15, 49–67, <https://doi.org/10.1016/j.ejrh.2017.11.005>, 2018.

467 Hancock, P. A. and Hutchinson, M.: Spatial interpolation of large climate data sets using bivariate thin
468 plate smoothing splines, *Environ. Modell. Softw.*, 21, 1684–1694,
469 <https://doi.org/10.1016/j.envsoft.2005.08.005>, 2006.

470 Hillman, A. L., Abbott, M. B., Finkenbinder, M. S., and Yu, J.: An 8,600 year lacustrine record of summer
471 monsoon variability from Yunnan, China, *Quaternary Sci. Rev.*, 174, 120–132,
472 <https://doi.org/10.1016/j.quascirev.2017.09.005>, 2017.

473 Hillman, A. L., O'Quinn, R. F., Abbott, M. B., and Bain, D. J.: A Holocene history of the Indian monsoon
474 from Qilu Lake, southwestern China, *Quaternary Sci. Rev.*, 227, 106051,
475 <https://doi.org/10.1016/j.quascirev.2019.106051>, 2020.

476 Hodell, D. A., Brenner, M., Kanfoush, S. L., Curtis, J. H., Stoner, J. S., Xueliang, S., Yuan, W., and
477 Whitmore, T. J.: Paleoclimate of southwestern China for the past 50,000 yr inferred from lake
478 sediment records, *Quaternary Res.*, 52, 369–380, <https://doi.org/10.1006/qres.1999.2072>, 1999.

479 Huang, C., Wei, G., Ma, J., and Liu, Y.: Evolution of the Indian summer monsoon during the interval 32.7–

480 11.4 cal. ka BP: Evidence from the Baoxiu peat, Yunnan, southwest China, *J. Asian Earth Sci.*, 131,
481 72–80, <https://doi.org/10.1016/j.jseaes.2016.09.008>, 2016.

482 Hutchinson, M. (Ed.): ANUSPLIN version 4.36 user guide, Centre for Resource and Environmental
483 Studies, the Australian National University, Canberra, Canada, 2006.

484 Juggins, S.: rioja: Analysis of Quaternary Science Data, R package version (0.9-15.1) [code], [http://cran.r-](http://cran.r-project.org/package=rioja)
485 [project.org/package=rioja](http://cran.r-project.org/package=rioja), 2017.

486 Lawrence, D. M. and Slingo, J. M.: An annual cycle of vegetation in a GCM. Part I: implementation and
487 impact on evaporation, *Clim. Dynam.*, 22, 87–105, <http://doi.org/10.1007/s00382-003-0366-9>, 2004.

488 Leng, M. J. and Marshall, J. D.: Palaeoclimate interpretation of stable isotope data from lake sediment
489 archives, *Quaternary Sci. Rev.*, 23, 811–831, <https://doi.org/10.1016/j.quascirev.2003.06.012>, 2004.

490 Li, Y., Chen, X., Xiao, X., Zhang, H., Xue, B., Shen, J., and Zhang, E.: Diatom-based inference of Asian
491 monsoon precipitation from a volcanic lake in southwest China for the last 18.5 ka, *Quaternary Sci.*
492 *Rev.*, 182, 109–120, <https://doi.org/10.1016/j.quascirev.2017.11.021>, 2018.

493 Luo, C., Zheng, Z., Tarasov, P., Pan, A., Huang, K., Beaudouin, C., and An, F.: Characteristics of the
494 modern pollen distribution and their relationship to vegetation in the Xinjiang region, northwestern
495 China, *Rev. Palaeobot. Palyno.*, 153, 282–295, <https://doi.org/10.1016/j.revpalbo.2008.08.007>, 2009.

496 Markewitz, D., Devine, S., Davidson, E. A., Brando, P., and Nepstad, D. C.: Soil moisture depletion under
497 simulated drought in the Amazon: impacts on deep root uptake, *New Phytol.*, 187, 592–607,
498 <https://doi.org/10.1111/j.1469-8137.2010.03391.x>, 2010.

499 Maxwell, R. M. and Condon, L. E.: Connections between groundwater flow and transpiration partitioning,
500 *Science*, 353, 377–380, <http://doi.org/10.1126/science.aaf7891>, 2016.

501 Mishra, A. K. and Singh, V. P.: A review of drought concepts, *J. Hydrol.*, 391, 202–216,
502 <https://doi.org/10.1016/j.jhydrol.2010.07.012>, 2010.

503 Mohammad, A. G. and Adam, M. A.: The impact of vegetative cover type on runoff and soil erosion under
504 different land uses, *Catena*, 81, 97–103, <https://doi.org/10.1016/j.catena.2010.01.008>, 2010.

505 Ni, J., Cao, X., Jeltsch, F., and Herzschuh, U.: Biome distribution over the last 22,000 yr in China,
506 *Palaeogeogra. Palaeocl.*, 409, 33–47, <https://doi.org/10.1016/j.palaeo.2014.04.023>, 2014.

507 Ning, D., Zhang, E., Sun, W., Chang, J., and Shulmeister, J.: Holocene Indian Summer Monsoon variation
508 inferred from geochemical and grain size records from Lake Ximenglongtan, southwestern China,
509 *Palaeogeogra. Palaeocl.*, 487, 260–269, <https://doi.org/10.1016/j.palaeo.2017.09.008>, 2017.

510 Ohlendorf, C., Fey, M., Gebhardt, C., Haberzettl, T., Lücke, A., Mayr, C., Schäbitz, F., Wille, M., and
511 Zolitschka, B.: Mechanisms of lake-level change at Laguna Potrok Aike (Argentina)—insights from
512 hydrological balance calculations, *Quaternary Sci. Rev.*, 71, 27–45,
513 <https://doi.org/10.1016/j.quascirev.2012.10.040>, 2013.

514 Peng, J., Yang, X., Toney, J. L., Ruan, J., Li, G., Zhou, Q., Gao, H., Xie, Y., Chen, Q., and Zhang, T.: Indian
515 Summer Monsoon variations and competing influences between hemispheres since ~35 ka recorded
516 in Tengchongqinghai Lake, southwestern China, *Palaeogeogra. Palaeocl.*, 516, 113–125,
517 <https://doi.org/10.1016/j.palaeo.2018.11.040>, 2019.

518 Peng, Y., Xiao, J., Nakamura, T., Liu, B., and Inouchi, Y.: Holocene East Asian monsoonal precipitation
519 pattern revealed by grain-size distribution of core sediments of Daihai Lake in Inner Mongolia of north-
520 central China, *Earth Planet. Sc. Lett.*, 233, 467–479, <https://doi.org/10.1016/j.epsl.2005.02.022>, 2005.

521 Pokhrel, Y., Felfelani, F., Satoh, Y., Boulange, J., Burek, P., Gädeke, A., Gerten, D., Gosling, S. N., Grillakis,
522 M., and Gudmundsson, L.: Global terrestrial water storage and drought severity under climate change,
523 *Nat. Clim. Change*, 11, 226–233, <https://doi.org/10.1038/s41558-020-00972-w>, 2021.

524 Prentice, I. C.: Multidimensional scaling as a research tool in Quaternary palynology: a review of theory
525 and methods, *Rev. Palaeobot. Palyno.*, 31, 71–104, [https://doi.org/10.1016/0034-6667\(80\)90023-8](https://doi.org/10.1016/0034-6667(80)90023-8),
526 1980.

527 Prentice, I. C., Sykes, M. T., and Cramer, W.: A simulation model for the transient effects of climate change
528 on forest landscapes, *Ecol. Model.*, 65, 51–70, [https://doi.org/10.1016/0304-3800\(93\)90126-D](https://doi.org/10.1016/0304-3800(93)90126-D), 1993.

529 Qiu, J.: China drought highlights future climate threats: Yunnan's worst drought for many years has been
530 exacerbated by destruction of forest cover and a history of poor water management, *Nature*, 465,
531 142–144, <http://doi.org/10.1038/465142a>, 2010.

532 R Core Team: R: A language and environment for statistical computing., R Foundation for Statistical
533 Computing [code], <https://www.R-project.org/>, 2018.

534 Raidt, H. and Koschel, R.: Morphology of calcite crystals in hardwater lakes, *Limnologica*, 19, 3–12, 1988.

535 Reimer, P. J., Austin, W. E. N., Bard, E., Bayliss, A., Blackwell, P. G., Ramsey, C. B., Butzin, M., Cheng,
536 H., Edwards, R. L., Friedrich, M., Grootes, P. M., Guilderson, T. P., Hajdas, I., Heaton, T. J., Hogg, A.
537 G., Hughen, K. A., Kromer, B., Manning, S. W., Muscheler, R., Palmer, J. G., Pearson, C., van der
538 Plicht, J., Reimer, R. W., Richards, D. A., Scott, E. M., Southon, J. R., Turney, C. S. M., Wacker, L.,
539 Adolphi, F., Büntgen, U., Capano, M., Fahrni, S. M., Fogtmann-Schulz, A., Friedrich, R., Köhler, P.,

540 Kudsk, S., Miyake, F., Olsen, J., Reinig, F., Sakamoto, M., Sookdeo, A., and Talamo, S.: The IntCal20
541 Northern Hemisphere radiocarbon age calibration curve (0–55 kcal BP), *Radiocarbon*, 62, 725–757,
542 <http://doi.org/10.1017/RDC.2020.41>, 2020.

543 Robbins, L. and Blackwelder, P.: Biochemical and ultrastructural evidence for the origin of whittings: A
544 biologically induced calcium carbonate precipitation mechanism, *Geology*, 20, 464–468,
545 [http://doi.org/10.1130/0091-7613\(1992\)020<0464:BAUEFT>2.3.CO;2](http://doi.org/10.1130/0091-7613(1992)020<0464:BAUEFT>2.3.CO;2), 1992.

546 Scheff, J., Seager, R., Liu, H., and Coats, S.: Are glacials dry? Consequences for paleoclimatology and
547 for greenhouse warming, *J. Climate*, 30, 6593–6609, <https://doi.org/10.1175/JCLI-D-16-0854.1>, 2017.

548 Schlesinger, W. H. and Jasechko, S.: Transpiration in the global water cycle, *Agr. Forest Meteorol.*, 189,
549 115–117, <https://doi.org/10.1016/j.agrformet.2014.01.011>, 2014.

550 Sheng, E., Yu, K., Xu, H., Lan, J., Liu, B., and Che, S.: Late holocene Indian summer monsoon
551 precipitation history at Lake Lugu, northwestern Yunnan Province, southwestern China,
552 *Palaeogeogra. Palaeocl.*, 438, 24–33, <https://doi.org/10.1016/j.palaeo.2015.07.026>, 2015.

553 Stabel, H.-H.: Calcite precipitation in Lake Constance: Chemical equilibrium, sedimentation, and
554 nucleation by algae, *Limnol. Oceanogr.*, 31, 1081–1093, <https://doi.org/10.4319/lo.1986.31.5.1081>,
555 1986.

556 Sun, S., Chen, H., Ju, W., Wang, G., Sun, G., Huang, J., Ma, H., Gao, C., Hua, W., and Yan, G.: On the
557 coupling between precipitation and potential evapotranspiration: contributions to decadal drought
558 anomalies in the Southwest China, *Clim. Dynam.*, 48, 3779–3797, [http://doi.org/10.1007/s00382-](http://doi.org/10.1007/s00382-016-3302-5)
559 [016-3302-5](http://doi.org/10.1007/s00382-016-3302-5), 2017.

560 Sun, W., Zhang, E., Shulmeister, J., Bird, M. I., Chang, J., and Shen, J.: Abrupt changes in Indian summer
561 monsoon strength during the last deglaciation and early Holocene based on stable isotope evidence
562 from Lake Chenghai, southwest China, *Quaternary Sci. Rev.*, 218, 1–9,
563 <https://doi.org/10.1016/j.quascirev.2019.06.006>, 2019.

564 ter Braak, C. J. and Juggins, S.: Weighted averaging partial least squares regression (WA-PLS): an
565 improved method for reconstructing environmental variables from species assemblages, Twelfth
566 international diatom symposium, Renesse, The Netherlands, <http://doi.org/10.1007/BF00028046>,
567 1993.

568 The Editorial Committee of Vegetation Map of China, Chinese Academy of Sciences (Ed.): *Vegetation*
569 *Map of the People's Republic of China (1:1 000 000)*, Geology Press, Beijing, 2007.

570 Trenberth, K. E., Dai, A., Van Der Schrier, G., Jones, P. D., Barichivich, J., Briffa, K. R., and Sheffield, J.:
571 Global warming and changes in drought, *Nat. Clim. Change*, 4, 17–22,
572 <https://doi.org/10.1038/nclimate2067>, 2014.

573 Wang, G., Wang, Y., Wei, Z., He, W., Ma, X., and Zhang, T.: Reconstruction of temperature and
574 precipitation spanning the past 28 kyr based on branched tetraether lipids from Qionghai Lake,
575 southwestern China, *Palaeogeogra. Palaeocl.*, 562, 110094,
576 <https://doi.org/10.1016/j.palaeo.2020.110094>, 2020.

577 Wang, G., Wang, Y., Wei, Z., He, W., Ma, X., Sun, Z., Xu, L., Gong, J., Wang, Z., and Pan, Y.: Paleoclimate
578 changes of the past 30 cal ka BP inferred from lipid biomarkers and geochemical records from
579 Qionghai Lake, southwest China, *J. Asian Earth Sci.*, 172, 346–358,
580 <https://doi.org/10.1016/j.jseaes.2018.09.019>, 2019.

581 Wang, L., Yuan, X., Xie, Z., Wu, P., and Li, Y.: Increasing flash droughts over China during the recent
582 global warming hiatus, *Scientific Reports*, 6, 30571, <https://doi.org/10.1038/srep30571>, 2016.

583 Wang, S. and Dou, H. (Eds.): *The lake inventory of China*, Science Press, Beijing, 1998.

584 Watras, C., Read, J., Holman, K., Liu, Z., Song, Y. Y., Watras, A., Morgan, S., and Stanley, E.: Decadal
585 oscillation of lakes and aquifers in the upper Great Lakes region of North America: Hydroclimatic
586 implications, *Geophys. Res. Lett.*, 41, 456–462, <https://doi.org/10.1002/2013GL058679>, 2014.

587 Wei, G., Xie, L., Sun, Y., Lu, Y., and Liu, Y.: Major and trace elements of a peat core from Yunnan,
588 Southwest China: implications for paleoclimatic proxies, *J. Asian Earth Sci.*, 58, 64–77,
589 <https://doi.org/10.1016/j.jseaes.2012.06.021>, 2012.

590 Whitmore, T. J., Brenner, M., Jiang, Z., Curtis, J. H., Moore, A., Engstrom, D. R., and Wu, Y.: Water quality
591 and sediment geochemistry in lakes of Yunnan Province, southern China, *Environ. Geol.*, 32, 45–55,
592 <https://doi.org/10.1007/s002540050192>, 1997.

593 Wu, D., Zhou, A., Liu, J., Chen, X., Wei, H., Sun, H., Yu, J., Bloemendal, J., and Chen, F.: Changing
594 intensity of human activity over the last 2,000 years recorded by the magnetic characteristics of
595 sediments from Xingyun Lake, Yunnan, China, *J. Paleolimnol.*, 53, 47–60,
596 <http://doi.org/10.1007/s10933-014-9806-2>, 2015.

597 Wu, D., Chen, X., Lv, F., Brenner, M., Curtis, J., Zhou, A., Chen, J., Abbott, M., Yu, J., and Chen, F.:
598 Decoupled early Holocene summer temperature and monsoon precipitation in southwest China,
599 *Quaternary Sci. Rev.*, 193, 54–67, <https://doi.org/10.1016/j.quascirev.2018.05.038>, 2018.

600 Xiao, J., Fan, J., Zhou, L., Zhai, D., Wen, R., and Qin, X.: A model for linking grain-size component to lake
601 level status of a modern clastic lake, *J. Asian Earth Sci.*, 69, 149–158,
602 <https://doi.org/10.1016/j.jseaes.2012.07.003>, 2013.

603 Xiao, X., Haberle, S. G., Shen, J., Xue, B., Burrows, M., and Wang, S.: Postglacial fire history and
604 interactions with vegetation and climate in southwestern Yunnan Province of China, *Clim. Past*, 13,
605 613–627, <https://doi.org/10.5194/cp-13-613-2017>, 2017.

606 Xiao, X., Haberle, S. G., Yang, X., Shen, J., Han, Y., and Wang, S.: New evidence on deglacial climatic
607 variability from an alpine lacustrine record in northwestern Yunnan Province, southwestern China,
608 *Palaeogeogr. Palaeoclimatol.*, 406, 9–21, <https://doi.org/10.1016/j.palaeo.2014.04.008>, 2014a.

609 Xiao, X., Haberle, S. G., Shen, J., Yang, X., Han, Y., Zhang, E., and Wang, S.: Latest Pleistocene and
610 Holocene vegetation and climate history inferred from an alpine lacustrine record, northwestern
611 Yunnan Province, southwestern China, *Quaternary Sci. Rev.*, 86, 35–48,
612 <https://doi.org/10.1016/j.quascirev.2013.12.023>, 2014b.

613 Xiao, X., Haberle, S. G., Li, Y., Liu, E., Shen, J., Zhang, E., Yin, J., and Wang, S.: Evidence of Holocene
614 climatic change and human impact in northwestern Yunnan Province: High-resolution pollen and
615 charcoal records from Chenghai Lake, southwestern China, *Holocene*, 28, 127–139,
616 <https://doi.org/10.1177/0959683617715692>, 2018.

617 Xu, H., Lan, J., Zhang, G., and Zhou, X.: Arid Central Asia saw mid-Holocene drought, *Geology*, 47, 255–
618 258, <https://doi.org/10.1130/G45686.1>, 2019.

619 Xu, Q., Li, Y., Yang, X., and Zheng, Z.: Quantitative relationship between pollen and vegetation in northern
620 China, *Sci. China Ser. D*, 50, 582–599, <http://doi.org/10.1007/s11430-007-2044-y>, 2007.

621 Zhang, E., Chang, J., Shulmeister, J., Langdon, P., Sun, W., Cao, Y., Yang, X., and Shen, J.: Summer
622 temperature fluctuations in Southwestern China during the end of the LGM and the last deglaciation,
623 *Earth Planet. Sc. Lett.*, 509, 78–87, <https://doi.org/10.1016/j.epsl.2018.12.024>, 2019a.

624 Zhang, E., Chang, J., Cao, Y., Sun, W., Shulmeister, J., Tang, H., Langdon, P. G., Yang, X., and Shen, J.:
625 Holocene high-resolution quantitative summer temperature reconstruction based on subfossil
626 chironomids from the southeast margin of the Qinghai-Tibetan Plateau, *Quaternary Sci. Rev.*, 165,
627 1–12, <https://doi.org/10.1016/j.quascirev.2017.04.008>, 2017.

628 Zhang, L., Zhang, H., Chang, F., Duan, L., Hu, J., Li, T., Cai, M., and Zhang, Y.: Spatial variation
629 characteristics of sediment size and its environmental indication significance in Lake Yilong, Yunnan

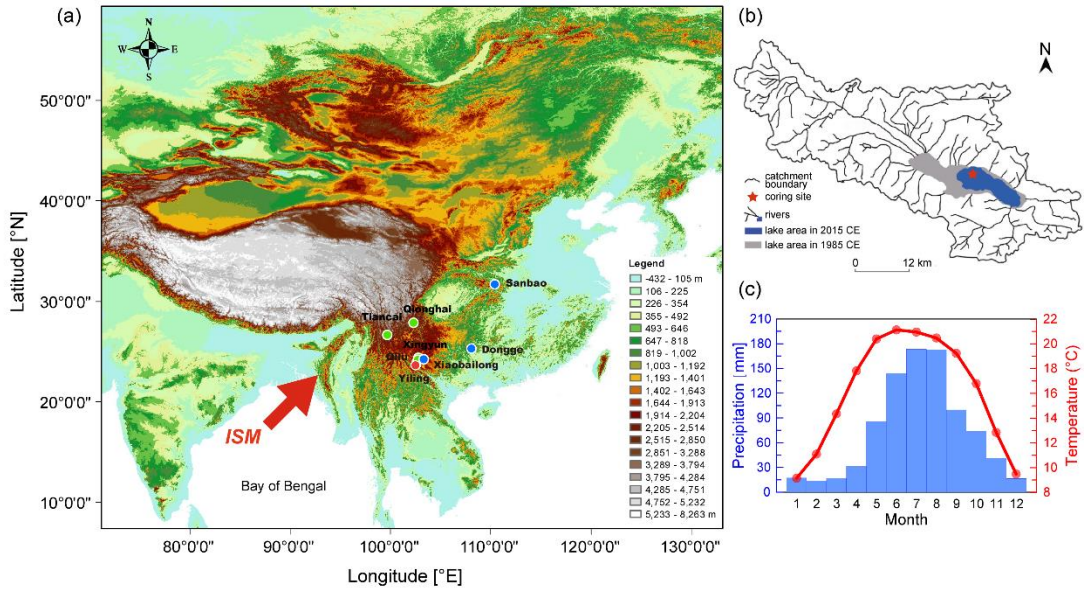
630 Province, *Quaternary Sci.*, 39, 1159–1170, <http://doi.org/10.11928/j.issn.1001-7410.2019.05.08>,
631 2019b. (in Chinese, with English abstract)

632 Zhang, Y.-K. and Schilling, K.: Effects of land cover on water table, soil moisture, evapotranspiration, and
633 groundwater recharge: a field observation and analysis, *J. Hydrol.*, 319, 328–338,
634 <https://doi.org/10.1016/j.jhydrol.2005.06.044>, 2006.

635 Zhao, M., Li, H.-C., Liu, Z.-H., Mii, H.-S., Sun, H.-L., Shen, C.-C., and Kang, S.-C.: Changes in climate
636 and vegetation of central Guizhou in southwest China since the last glacial reflected by stalagmite
637 records from Yelang Cave, *J. Asian Earth Sci.*, 114, 549–561,
638 <https://doi.org/10.1016/j.jseaes.2015.07.021>, 2015.

639

640



641

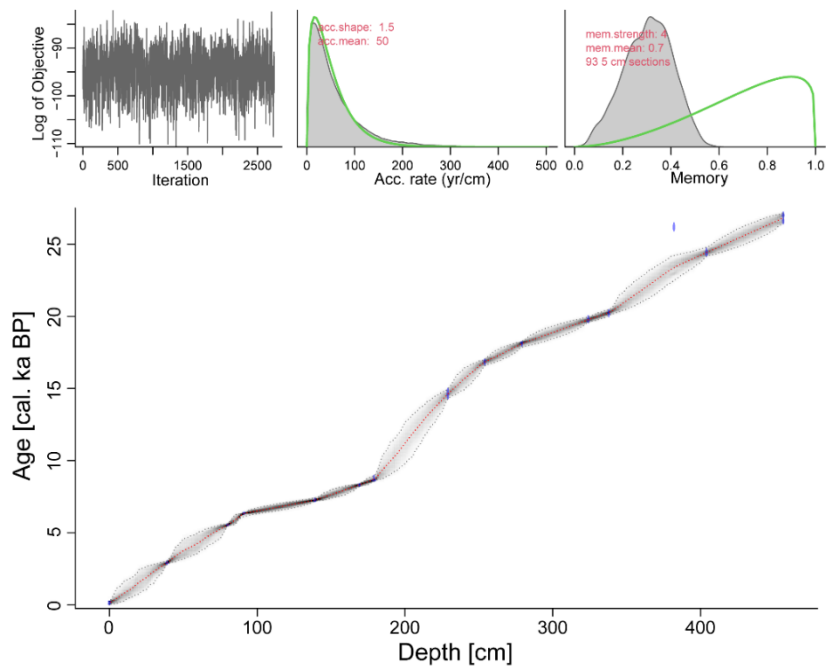
642 **Figure 1** (a) Map showing the location of Yilong Lake and other paleoclimatic records; (b)

643 catchment of the lake and the location of the core YLH; (c) average monthly temperature and

644 precipitation from 1951 to 2017 CE (China Meteorological Data Service Centre,

645 <https://data.cma.cn/en>).

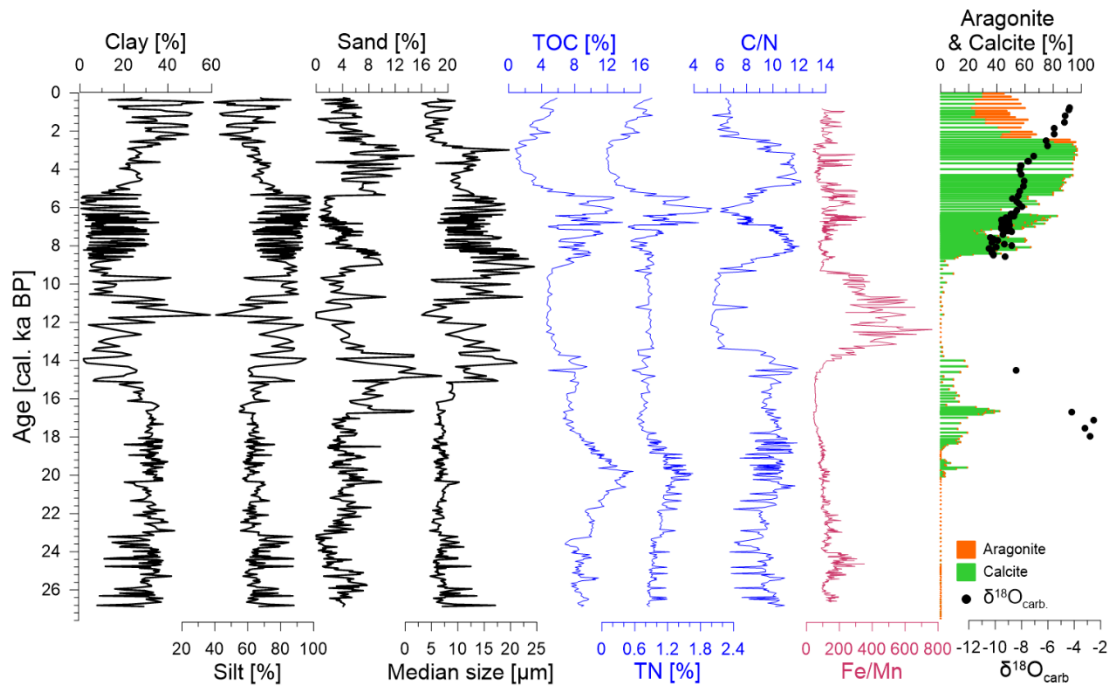
646



647

648

Figure 2 Age-depth model of the sediment core YLH.

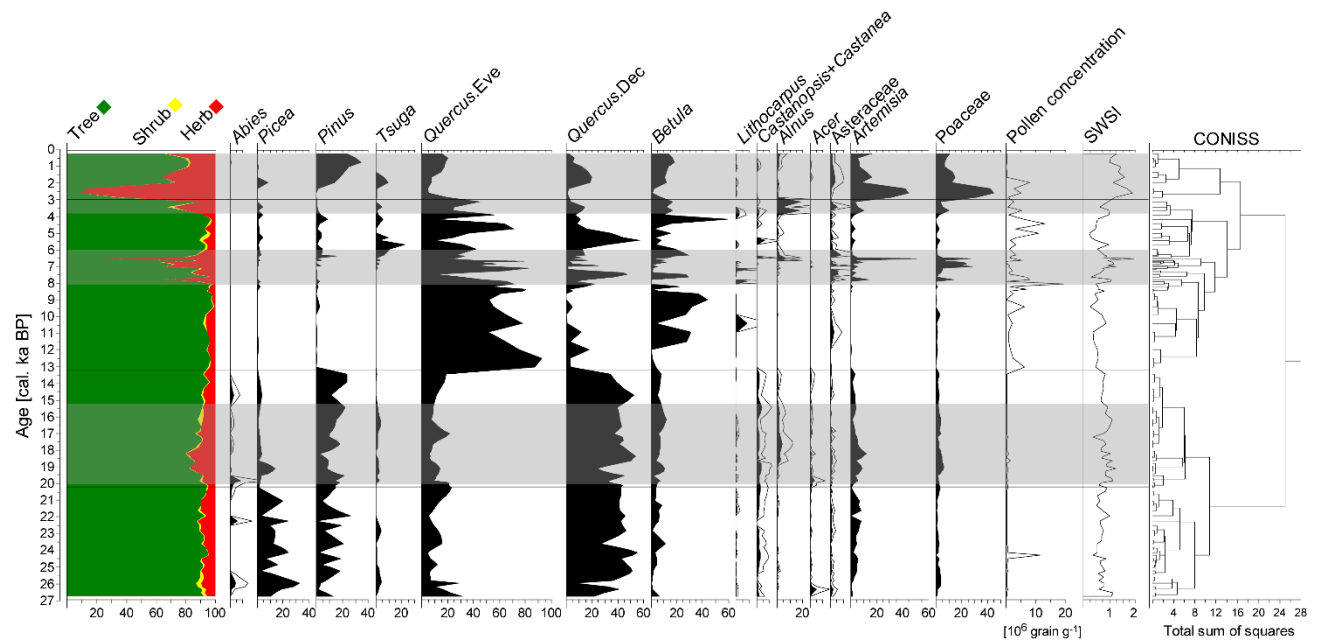


649

650 **Figure 3** Down-core variations in the grain-size components (clay, silt and sand), median grain

651 size, TOC and TN content, C/N and Fe/Mn ratios, calcite and aragonite content, and $\delta^{18}\text{O}_{\text{carb}}$.

652



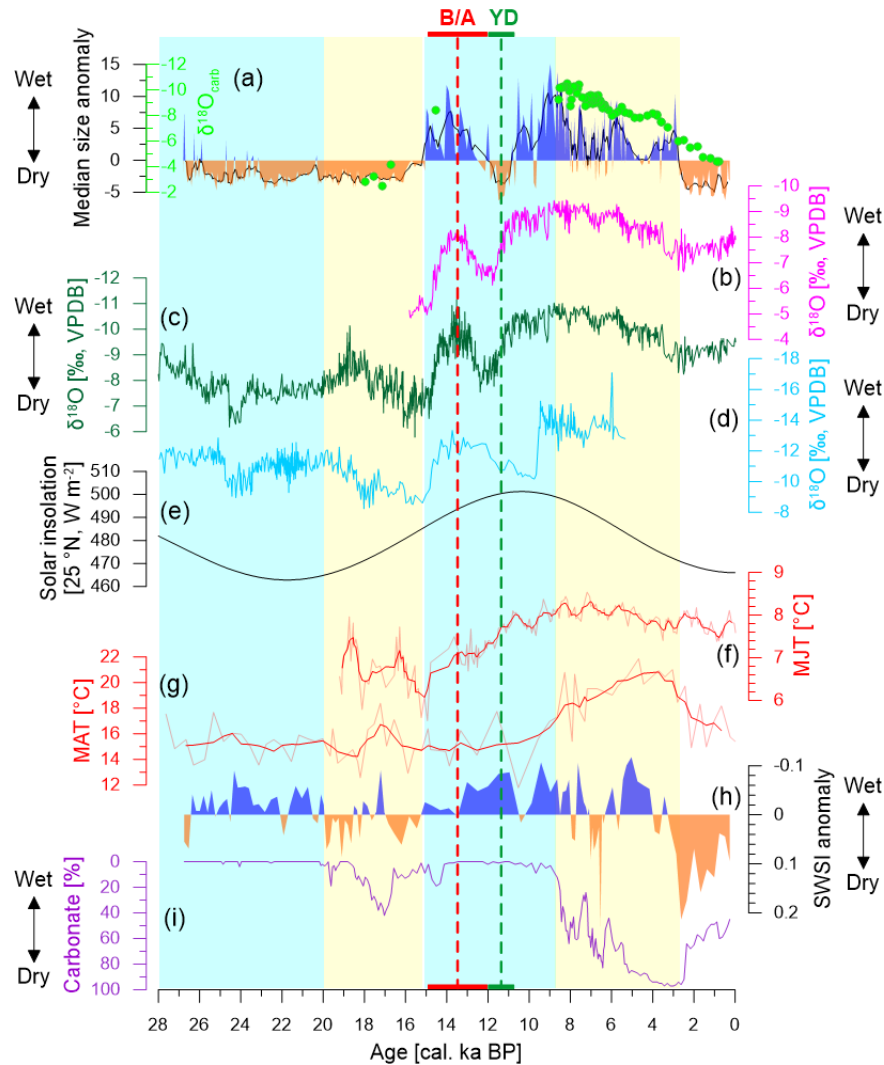
653

654 **Figure 4** Pollen percentages diagram of the main taxa (average percentages $\geq 5\%$), the

655 pollen concentration and the reconstructed soil water stress index (SWSI). Pollen types with

656 relatively low percentages have been magnified 3 times. Gray shadows mark periods of

657 relatively high SWSI.



659

660 **Figure 5** Median size and $\delta^{18}\text{O}_{\text{carb}}$ values from Yilong Lake (a); Stalagmite $\delta^{18}\text{O}$ records from
 661 Sanbao Cave (Cheng et al., 2016) (b), Dongge Cave (Dykoski et al., 2005) (c) and Xiaobailong
 662 Cave (Cai et al., 2015) (d); summer insolation curve for 25°N (e); chironomid-mean July
 663 temperature (MJT) from Tiancai Lake (Zhang et al., 2019a) (f); brGDGT-derived mean annual
 664 temperature (MAT) from Qionghai Lake (Wang et al., 2020) (g); pollen-based reconstructed soil
 665 water stress index (SWSI) for Yilong region (h); carbonate content of sediments from Yilong
 666 Lake (i). Light yellow (blue) shadows denote periods of inconsistency (consistency) of dry/wet
 667 condition among precipitation, SWSI and hydrological balance.

668

Table 1 AMS ^{14}C results from the YLH sediment core.

Lab ID	Depth [cm]	Materials	IRMS $\delta^{13}\text{C}$ [‰]	Conventional Radiocarbon Age [yr BP]	Calibrated Age [2 σ , cal. yr BP]
Beta-468347	1	Sediment-TOC	24.6	-30 +/- 30	100.37 +/- 0.37 pMC
Beta-492284	40	Charcoal and plant remains	-21.5	2820 +/- 30	2848–3004
Beta-492285	80	Charcoal and plant remains	-20	4820 +/- 30	5477–5539
Beta-468348	91	Sediment-TOC	-27.3	5560 +/- 30	6297–6398
Beta-492286	140	Charcoal and plant remains	-18.7	6330 +/- 30	7237–7318
Beta-468349	170	Charcoal and plant remains	-21.5	7510 +/- 30	8289–8386
Beta-492287	180	Charcoal and plant remains	-28.7	7860 +/- 30	8585–8771
Beta-492288	230	Charcoal and plant remains	-13.1	12460 +/- 40	14322–14745
Beta-468350	255	Sediment-TOC	-17.6	13880 +/- 40	16678–17025
Beta-492289	280	Sediment-TOC	-18.8	14800 +/- 40	17986–18242
Beta-468351	325	Sediment-TOC	-19.9	16400 +/- 50	19582–19923
Beta-541605	338	Plant remains	-27	16730 +/- 50	20058–20408
Beta-468352	383	Sediment-TOC	-19.3	21980 +/- 70	25973–26393
Beta-537522	404	Charcoal	-25.1	20320 +/- 70	24183–24631
Beta-468353	457	Plant remains	-17.8	22560 +/- 80	26829–27171